Sensitivity analysis of the leading global modes of the flow around a NACA 4412 airfoil

Gabriele Nastro, Jean-Christophe Robinet, Jean-Christophe Loiseau, Pierre-Yves Passaggia, Lucien Baldas, Nicolas Mazellier, Bruno Stefes

Sensitivity analysis of the leading global modes of the flow around a NACA 4412 airfoil

Gabriele Nastro*
University of Orléans, INSA-CVL, PRISME, EA 4229, 45072 Orléans, France
Arts et Métiers Institute of Technology, CNAM, DynFluid, HESAM Université, F-75013 Paris, France

Jean-Christophe Robinet†
Arts et Métiers Institute of Technology, CNAM, DynFluid, HESAM Université, F-75013 Paris, France

Jean-Christophe Loiseau‡
Arts et Métiers Institute of Technology, CNAM, DynFluid, HESAM Université, F-75013 Paris, France

Pierre-Yves Passaggia§
University of Orléans, INSA-CVL, PRISME, EA 4229, 45072 Orléans, France

Lucien Baldas¶
Institut Clément Ader (ICA), Université de Toulouse, CNRS, INSA, ISAE-SUPAERO, Mines-Albi, UPS, Toulouse, France

Nicolas Mazellier‖
University of Orléans, INSA-CVL, PRISME, EA 4229, 45072 Orléans, France

Bruno Stefes
Airbus Operations GmbH, Bremen, Germany

Two- and three-dimensional modes developing on a steady spanwise-homogeneous laminar separated flow over a NACA 4412 airfoil have been numerically investigated using global linear stability theory. Considering variations of both the Reynolds number and the angle of attack, the two-dimensional von Kármán mode results to be always the leading mode since for all conditions examined it is more unstable than the three-dimensional von Kármán modes and the three-dimensional stationary modes, associated with the formation on the airfoil surface of large-scale separation patterns akin to stall cells. Sensitivity of the global modes is investigated numerically through adjoint-based methods in order to predict regions of the flow which are most sensitive to a modification of the base flow and the application of a steady force. Interestingly, the instability's growth rate sensitivity function displays an extended region upstream of the separation bubble wherein a streamwise oriented force has a net stabilizing effect. Aerodynamic performances can thus be possibly improved by leveraging the boat-tailing effect induced by tangential jet actuators localized in this particular region of the flow.

Nomenclature

c	=	chord of the airfoil
U_∞	=	free-stream velocity
$\boldsymbol{q} = (\boldsymbol{u}, p)$	=	state vector
$\boldsymbol{f}$	=	body force

*Postdoc, Laboratoire PRISME & Laboratoire DynFluid, gabriele.nastro@univ-orleans.fr
†Professor, Laboratoire DynFluid, jean-christophe.robinet@ensam.eu
‡Professor, Laboratoire DynFluid, jean-christophe.loiseau@ensam.eu
§Professor, Laboratoire PRISME, pierre-yves.passaggia@univ-orleans.fr
¶Professor, Institut Clément Ader, baldas@insa-toulouse.fr
‖Professor, Laboratoire PRISME, nicolas.mazellier@univ-orleans.fr

Re	=	Reynolds number
ν	=	kinematic viscosity of the fluid
α	=	angle of attack
St	=	Strouhal number
$\boldsymbol{Q} = (\boldsymbol{U}, P)$	=	base flow
$\boldsymbol{q}' = (\boldsymbol{u}', p')$	=	direct mode
c.c.	=	complex conjugate
$\sigma = \lambda + \mathrm{i}\omega$	=	eigenvalue
λ	=	growth rate
ω	=	angular frequency
Ω	=	control volume
$\boldsymbol{q}^\dagger = (\boldsymbol{u}^\dagger, p^\dagger)$	=	adjoint mode
$\boldsymbol{Q}^\dagger = (\boldsymbol{U}^\dagger, P^\dagger)$	=	adjoint base flow
β	=	spanwise wavenumber

I. Introduction

TAKE off and landing are critical phases of flight during which close to 60% of fatal accidents happen. During these maneuvers, characterized by relatively large angles of attack, the use of complex wing geometries optimized for cruise flight can lead to the formation of a massively separated flow region on the suction side of the wing. This reversed flow region causes a large increase of the drag exerted on the wing and can possibly induce stall, a major limiting cause for rapid take off and climbing to cruise altitude. Designing efficient control strategies to mitigate these issues is thus critical. In this context, the H2020 Clean-Sky project *PERSEUS*, involving several French academic research laboratories along with Airbus, thus aims at designing active flow-control strategies based on Pulsed Jet Actuators (PJAs) and testing these on a wind-tunnel model at large Reynolds numbers. In particular, we aim at designing pulsed jet actuators that can easily be embedded in the leading edge of the wing model and at determining a control strategy suppressing separation while simultaneously minimizing the net mass-flow rate used for this control.

To this end, the aim of the present contribution is to develop state-of-the-art sensitivity analyses to guide the placement of these actuators. For that purpose, adjoint-based sensitivity methods [1] are implemented in the massively parallel spectral element code Nek5000 [2]. As proof of concept, these techniques are here applied to a wing modeled using a NACA4412 airfoil at low Reynolds numbers and angles of attack for which separation occurs. This analysis at low-Reynolds-number condition could help understand more complex mechanisms at higher Reynolds numbers, since the vortex shedding phenomenon governing the low Reynolds number dynamics persists at higher Reynolds numbers in the fully developed turbulent regime [3]. Such an approach can help at identifying regions of the flow most sensitive to an external force modeling the influence of the actuators. The resulting sensitivity maps thus provide guidelines for quasi-optimal actuator placement in order to quench the instability modes. In a similar context, previous studies on the canonical two-dimensional cylinder flow provided experimental [4] and numerical [1] evidences of the complete suppression of the vortex shedding phenomenon in the presence of a localized force such as the one induced by a small control cylinder.

The present paper is organized as follows. The mathematical framework is presented in Section II. Starting from the nonlinear incompressible Navier-Stokes equations, the linearized equations governing the dynamics of infinitesimal perturbations are first derived. These equations form the basis for the global linear stability analysis to be conducted in order to extract the instability modes driving the flow dynamics. In a second step, the adjoint-based framework used to investigate the sensitivity of this instability with respect to an external steady force is presented. We then focus on the flow around a NACA 4412 wing which is described in Section III, together with results from the stability and sensitivity analyses. Conclusions and perspectives are finally addressed and discussed in Section IV.

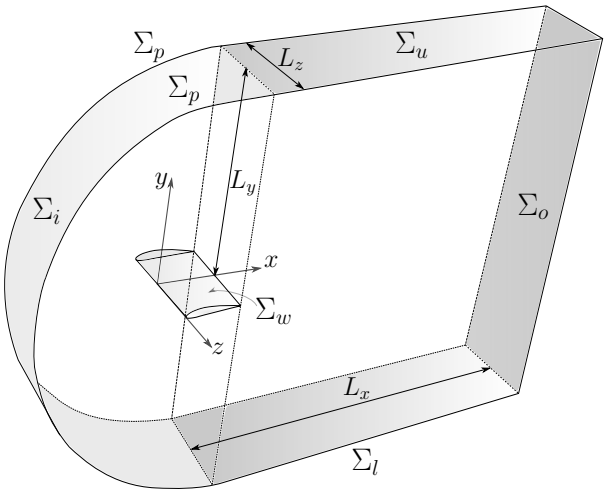

Fig. 1 Sketch of the geometry and the flow computational domain for the numerical simulations.

II. Formulation of the problem

A. Navier-Stokes simulations

The flow dynamics of an incompressible Newtonian fluid are governed by the following Navier-Stokes equations

$$\partial_t \boldsymbol{u} + \boldsymbol{u} \cdot \boldsymbol{\nabla} \boldsymbol{u} = -\boldsymbol{\nabla} p + \frac{1}{Re} \boldsymbol{\Delta} \boldsymbol{u} + \boldsymbol{f} \tag{1a}$$

$$\boldsymbol{\nabla} \cdot \boldsymbol{u} = 0 \tag{1b}$$

with $\boldsymbol{u}(\boldsymbol{x}, t) = (u, v, w)^T$ the velocity field and $p(\boldsymbol{x}, t)$ the pressure field, respectively, and $\boldsymbol{f}(\boldsymbol{x}, t)$ represents an external force. The Reynolds number is defined as

$$Re = \frac{U_\infty c}{\nu}$$

where U_∞ is the free-stream velocity, c the chord of the airfoil and ν the kinematic viscosity of the fluid. The origin of our Cartesian reference frame (x, y, z) is set at the leading edge of the airfoil, with x denoting the streamwise direction, y the cross-stream direction and z the spanwise direction, respectively. A sketch of the geometry and the computational domain is shown in Fig. 1. The Navier-Stokes equations are completed with the following boundary conditions: $\boldsymbol{u} = (U_\infty, 0, 0)$ at the inlet Σ_i, a stress-free boundary condition $p\boldsymbol{n} - Re^{-1} \nabla \boldsymbol{u} \cdot \boldsymbol{n} = 0$ at the outlet Σ_o, symmetry conditions on the lower and upper boundaries Σ_l and Σ_u, periodic conditions on the lateral boundaries Σ_p and no-slip conditions $\boldsymbol{u} = 0$ on the solid walls Σ_w (see Fig. 1b).

The Navier-Stokes equations are then solved numerically using the spectral element solver Nek5000 [2]. Spatial discretization relies on a C-grid mesh made of approximately 50 000 spectral elements with polynomial order $P = 6$ while a third-order accurate temporal scheme is used to integrate forward in time the equations. The streamwise and cross-stream extents are set to $L_x = 50$ and $L_y = 30$ respectively, while the spanwise one ranges from $L_z = 8$ to $L_z = 4\pi$. The same computational domain and numerical schemes are also used to compute the base flows as well as for conducting the linear stability and sensitivity analyses.

The dynamics of the flow are parametrized by the Reynolds number Re and the angle of attack α. Hereafter, the Reynolds number at which a specific steady equilibrium solution bifurcates to another equilibrium state for a fixed angle of attack will be referred to as the critical Reynolds number Re_{cr}. Similarly, the angle of attack at which this transition occurs for a fixed Reynolds number will be referred to as the critical angle of attack α_{cr}.

B. Base flow

Base flows are defined as being fixed points of the unsteady and nonlinear Navier-Stokes equations (1a) and (1b) and correspond to steady equilibrium solutions. Computing these particular solutions is thus a prerequisite for the stability and sensitivity analyses to be conducted in this study. However, because of the sheer size of the system of equations

involved, their computation remains an intensive task for realistic geometries whose complexity is further augmented by the use of general-purpose time-stepper CFD codes.

Over the years, various approaches have been proposed to tackle the computation of these (possibly unstable) steady solutions while requiring minimal modifications to an existing time-stepper code. One can cite for instance the *selective frequency damping* (SFD) proposed by Åkervik et al. [5] in 2006 wherein a steady state solution is obtained by damping the unstable frequency via the addition of a dissipative relaxation term proportional to the high-frequency content of the velocity oscillations [see Refs. 5, 6, for a comprehensive review]. Denoting by $\partial_t \boldsymbol{q} = \boldsymbol{f}(\boldsymbol{q})$ the original Navier-Stokes equations, the corresponding system of equations solved for SFD is given by

$$\begin{aligned}\partial_t \boldsymbol{q} &= \boldsymbol{f}(\boldsymbol{q}) - \chi\,(\boldsymbol{q} - \bar{\boldsymbol{q}})\\ \partial_t \bar{\boldsymbol{q}} &= \omega_c\,(\boldsymbol{q} - \bar{\boldsymbol{q}})\end{aligned}$$

where $\bar{\boldsymbol{q}}$ is the temporally-filtered solution and χ and ω_c are the gain and cut-off frequency of the applied first-order filter. As this system of equations is integrated forward in time, $\boldsymbol{q}$ and $\bar{\boldsymbol{q}}$ converge toward the same solution. At convergence, we thus have $\boldsymbol{q} = \bar{\boldsymbol{q}}$ and this system of equations reduces to the stationary Navier-Stokes equations. Hence, $\boldsymbol{q}$ converges toward the fixed point of the original equations. Alternatively, one can also use a time-stepper formulation of the Newton-GMRES algorithm as described in Dijkstra et al. [7] and Loiseau et al. [8]. In the present work, both approaches have been considered and lead to virtually identical base flows. Hereafter, these base flows will be denoted as $\boldsymbol{Q} = (\boldsymbol{U}, P)^T$.

C. Direct and adjoint linear stability analyses

The dynamics of an infinitesimal perturbation $\boldsymbol{q}'(\boldsymbol{x}, t) = (\boldsymbol{u}', p')^T$ evolving on top of the base flow solution $\boldsymbol{Q}(\boldsymbol{x}) = (\boldsymbol{U}, P)^T$ are dictated by the linearized Navier-Stokes equations

$$\partial_t \boldsymbol{u}' + \boldsymbol{u}' \cdot \boldsymbol{\nabla}\boldsymbol{U} + \boldsymbol{U} \cdot \boldsymbol{\nabla}\boldsymbol{u}' = -\boldsymbol{\nabla} p' + \frac{1}{Re}\boldsymbol{\Delta}\boldsymbol{u}' \tag{2a}$$

$$\boldsymbol{\nabla} \cdot \boldsymbol{u}' = 0. \tag{2b}$$

In the frame of modal stability analysis, the disturbances are sought under the following form

$$(u', v', w', p')(\boldsymbol{x}, t) = (\hat{u}, \hat{v}, \hat{w}, \hat{p})(\boldsymbol{x}) \exp(\sigma t) + \text{c.c.}, \tag{3}$$

where c.c. stands for the complex conjugate and $\sigma = \lambda + \mathrm{i}\omega$ is the complex eigenvalue with λ the growth rate and ω the angular frequency, i.e. the frequency $f = \omega/2\pi$. Substituting the normal mode ansatz (3) into the linearized Navier-Stokes equations Eq. (2a) and Eq. (2b), the above linear initial-value problem can be recast as the following generalized eigenvalue problem:

$$\sigma \hat{\boldsymbol{u}} = -\boldsymbol{\nabla}\hat{\boldsymbol{u}} \cdot \boldsymbol{U} - \boldsymbol{\nabla}\boldsymbol{U} \cdot \hat{\boldsymbol{u}} - \boldsymbol{\nabla}\hat{p} + Re^{-1}\boldsymbol{\Delta}\hat{\boldsymbol{u}}, \tag{4a}$$

$$0 = \boldsymbol{\nabla} \cdot \hat{\boldsymbol{u}}. \tag{4b}$$

The asymptotic temporal features of the perturbation are thus obtained from the least damped/most unstable eigenvalue. For instance, the imaginary part of the leading eigenvalue determines whether the fixed point leads to pitchfork or transcritic ($\omega = 0$) or a Hopf-type ($\omega \neq 0$) bifurcation. Moreover, if this leading eigenvalue has a positive real part, i.e. $\lambda > 0$, the amplitude of the associated eigenmode will grow exponentially fast in time and, consequently, the base flow is asymptotically unstable. On the other hand, if the real parts of all eigenvalues are negative, i.e. $\lambda_k < 0\ \forall k$, the base flow is asymptotically stable and all eigenmodes will be damped over time.

From a linear algebra point of view, the generalized eigenvalue problem can be written as

$$\sigma \boldsymbol{B}\hat{\boldsymbol{q}} = \boldsymbol{L}\hat{\boldsymbol{q}}$$

where $\boldsymbol{B}$ is a singular mass matrix enforcing that the velocity is an actual degree of freedom of the problem while the perturbation pressure field can be understood as a Lagrange multiplier to enforce the divergence constraint. The operator $\boldsymbol{L}$ then corresponds to the Jacobian of the Navier-Stokes equations. Introducing a spatial inner product between two arbitrary state vectors $\boldsymbol{q}_1$ and $\boldsymbol{q}_2$

$$\langle \boldsymbol{q}_1 | \boldsymbol{q}_2 \rangle = \int_\Omega \boldsymbol{q}_1^* \boldsymbol{B} \boldsymbol{q}_2 \, \mathrm{d}\Omega$$

where Ω is the flow domain and the superscript * stands for the complex conjugate, one can introduce a so-called *adjoint Navier-Stokes operator* [9] satisfying

$$\langle \boldsymbol{q}_1 | \boldsymbol{L}\boldsymbol{q}_2 \rangle = \langle \boldsymbol{L}^\dagger \boldsymbol{q}_1 | \boldsymbol{q}_2 \rangle.$$

The corresponding adjoint eigenproblem then reads

$$\sigma^* \boldsymbol{u}^\dagger = \boldsymbol{\nabla}\boldsymbol{u}^\dagger \cdot \boldsymbol{U} - (\boldsymbol{\nabla}\boldsymbol{U})^T \cdot \boldsymbol{u}^\dagger - \boldsymbol{\nabla} p^\dagger + Re^{-1}\boldsymbol{\Delta}\boldsymbol{u}^\dagger, \tag{5a}$$

$$0 = \boldsymbol{\nabla} \cdot \boldsymbol{u}^\dagger \tag{5b}$$

where $\boldsymbol{q}^\dagger = (\boldsymbol{u}^\dagger, p^\dagger)^T$ is the adjoint state vector. For a discussion about the boundary conditions for the adjoint operator, interested readers are referred to Barkley et al. [10]. Whilst this concept of adjoint has originated from the optimization theory, it has since been used quite extensively in the hydrodynamic community to study linear and nonlinear transient growth of perturbations [10, 11] or to identify the most receptive path to turbulence. Following Marquet et al. [1], the present use of the adjoint enables us to select the most stabilizing or destabilizing base flow modification or to map the sensitivity of the leading unstable mode with respect to the application of an external force modeling our actuators, a crucial point in our study.

D. Sensitivity analysis

The sensitivity analysis consists of assessing how a variable is modified by the variation of a physical quantity. In particular, this study focuses on the sensitivity of the leading global modes. In this regard, a first instrument of the sensitivity analysis is the determination of the wavemaker region, i.e. the so-called structural sensitivity first introduced by Giannetti and Luchini [12] in the framework of the global stability. The wavemaker is defined by the following relation:

$$\zeta(\boldsymbol{x}) = \frac{\|\hat{\boldsymbol{u}}\|\|\boldsymbol{u}^\dagger\|}{\langle \boldsymbol{u}^\dagger | \hat{\boldsymbol{u}} \rangle} \tag{6}$$

where $\|\cdot\|$ should be understood as the pointwise norm of the mode. It allows for identifying regions of the flow where generic structural modifications of the linearized Navier-Stokes operator lead to the strongest drift of the leading eigenvalue.

The sensitivity of a given eigenvalue to an arbitrary base-flow modification or to a force can be considered. The concept of sensitivity to a base flow modification has been originally introduced by Bottaro et al. [13] in a local framework and then extended in the global framework also to a body force by Marquet et al. [1]. The variations $\delta\sigma$ of the complex eigenvalue with respect to an arbitrary small-amplitude base flow modification $\boldsymbol{\delta U}$ can be formally related through the inner product definition:

$$\delta\sigma = \langle \boldsymbol{\nabla}_{\boldsymbol{U}}\sigma | \boldsymbol{\delta U} \rangle. \tag{7}$$

The specific form of the sensitivity $\boldsymbol{\nabla}_{\boldsymbol{U}}\sigma$ is derived by a Lagrangian-based approach [see App. A in Ref. 1, for a complete derivation] and reads

$$\boldsymbol{\nabla}_{\boldsymbol{U}}\sigma = -(\boldsymbol{\nabla}\hat{\boldsymbol{u}})^H \cdot \boldsymbol{u}^\dagger + \boldsymbol{\nabla}\boldsymbol{u}^\dagger \cdot \hat{\boldsymbol{u}}^*, \tag{8}$$

where the superscript ^{H} denotes the transconjugate. Note that $\boldsymbol{\nabla}_{\boldsymbol{U}}\sigma$ is a complex vector field and variations of the growth rate $\delta\lambda$ and frequency $\delta\omega$ are linked to $\delta\sigma$ via $\boldsymbol{\nabla}_{\boldsymbol{U}}\lambda = \mathrm{Re}(\boldsymbol{\nabla}_{\boldsymbol{U}}\sigma)$ and $\boldsymbol{\nabla}_{\boldsymbol{U}}\omega = -\mathrm{Im}(\boldsymbol{\nabla}_{\boldsymbol{U}}\sigma)$. It should be stressed that the base-flow modification $\boldsymbol{\delta U}$ is generic since $\boldsymbol{U} + \boldsymbol{\delta U}$ is not assumed to be a steady solution of the equations governing the base flow.

Analogously, the sensitivity to a force can be derived. In our study, the body force $\boldsymbol{F}$ is assumed to be steady and to solely act on the base flow. This assumption is supported by the fact that the pulsed-jets-actuators' frequency is one order of magnitude larger than the flow natural frequency. Variations of a particular eigenvalue $\delta\sigma$ induced by infinitesimal variations $\boldsymbol{\delta F}$ of the body force are formally described by the following relation:

$$\delta\sigma = \langle \boldsymbol{\nabla}_{\boldsymbol{F}}\sigma | \boldsymbol{\delta F} \rangle, \tag{9}$$

where $\boldsymbol{\nabla}_{\boldsymbol{F}}\sigma$ defines the sensitivity to a steady force modification. As for the base flow sensitivity, $\boldsymbol{\nabla}_{\boldsymbol{F}}\sigma$ is a complex vector field so that $\boldsymbol{\nabla}_{\boldsymbol{F}}\lambda = \mathrm{Re}(\boldsymbol{\nabla}_{\boldsymbol{F}}\sigma)$ and $\boldsymbol{\nabla}_{\boldsymbol{F}}\omega = -\mathrm{Im}(\boldsymbol{\nabla}_{\boldsymbol{F}}\sigma)$. The Lagrangian-based approach allows to derive the following expression for the force sensitivity

$$\boldsymbol{\nabla}_{\boldsymbol{F}}\sigma = \boldsymbol{U}^\dagger, \tag{10}$$

where $\boldsymbol{Q}^\dagger = (\boldsymbol{U}^\dagger, P^\dagger)$ is the adjoint (complex) base flow whose governing equations read

$$-\boldsymbol{\nabla}\boldsymbol{U}^\dagger \cdot \boldsymbol{U} + (\boldsymbol{\nabla}\boldsymbol{U})^{\mathrm{T}} \cdot \boldsymbol{U}^\dagger - \boldsymbol{\nabla}P^\dagger - Re^{-1}\boldsymbol{\Delta}\boldsymbol{U}^\dagger = \boldsymbol{\nabla}_{\boldsymbol{U}}\sigma, \tag{11}$$

$$\boldsymbol{\nabla} \cdot \boldsymbol{U}^\dagger = 0. \tag{12}$$

Note that computing the force sensitivity $\boldsymbol{\nabla}_{\boldsymbol{F}}\sigma$ which is the focus of the present study requires the computation of the base flow sensitivity function beforehand.

III. Results

A. Navier-Stokes simulations

Depending on the initial condition, boundary conditions, and/or the value of the Reynolds number, the unforced Navier-Stokes equations may or may not allow for simulating a steady solution. For instance, Fig. 2 displaying the streamwise velocity u shows that for $\alpha = 20°$ and $Re = 400$ Eqs. (1a-1b) with $\boldsymbol{f} = \boldsymbol{0}$ are unstable since the flow experiences a Hopf bifurcation from a steady state towards a time-periodic nominally two-dimensional state in which two-dimensional vortices having their axes parallel to the one of the wing are shed. This transition from a

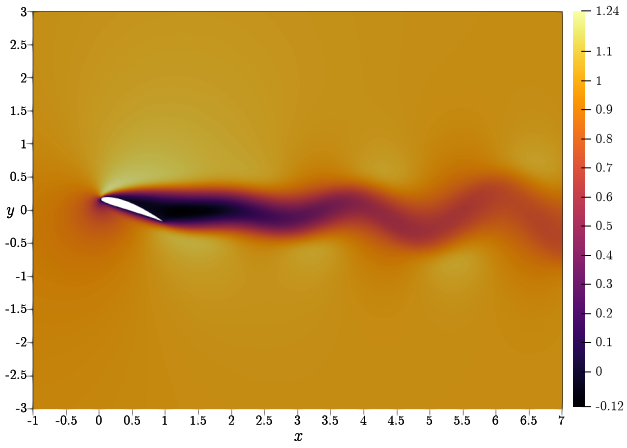

Fig. 2 Streamwise velocity distribution u around a NACA 4412 airfoil with $\alpha = 20°$ and $Re = 400$.

steady-to-time-periodic state is triggered by a global instability which is responsible for the onset of the so-called vortex shedding process. The Strouhal number given by the Fast-Fourier Transform on the nonlinear results is equal to $St \approx 0.5$.

B. Base flow

In order to apply the global stability approach, the base state for the same conditions presented above ($\alpha = 20°$ and $Re = 400$) is computed using the SFD method (see Section II.B) and illustrated in Fig. 3. This fixed point is thus adopted to compute the global mode responsible for the time-periodic state depicted by Fig. 2. It should be stressed that the stability analysis is only performed on the filtered base flow and, for such a base flow, the frequency of the most unstable mode accurately matches the natural vortex shedding frequency (i.e. the one obtainable from the nonlinear simulation) provided that the analysis is carried out under the stability threshold or in the vicinity of the bifurcation point.

C. Global stability analysis

We shall now apply the stability framework presented in Section II.C to the NACA 4412 wing. Figure 4(a) shows the spectrum relative to the base state of Fig. 3 for $\alpha = 20°$ and $Re = 400$. For these conditions, the most unstable global mode results to be the two-dimensional von Kármán (VK) mode with a frequency of 0.34. The difference between the flow natural frequency and the one obtained through the linear stability analysis is attributable to a strong distortion due to the nonlinear effects [14, 15]. As advocated above, it should be noted that this analysis is carried out far beyond the bifurcation threshold since the growth rate value is $\lambda = 0.412$ as shown in Fig. 4. In the unstable part of the spectrum below the 2D VK mode, we can distinguish the oblique VK modes and the so-called stall (ST) modes [16, 17]. Given ℓ

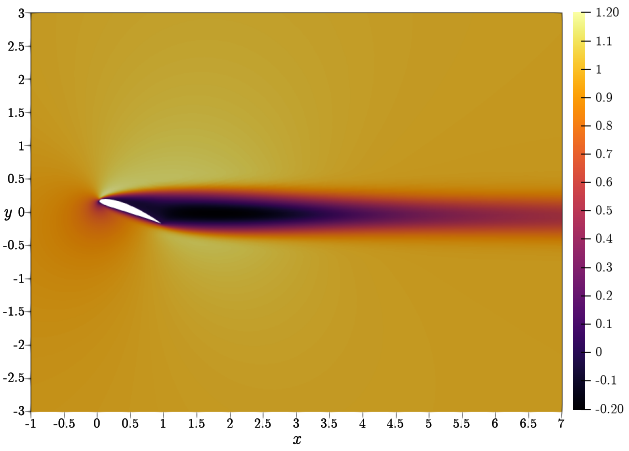

Fig. 3 Streamwise velocity distribution U of the base state for a NACA 4412 airfoil with $\alpha = 20°$ and $Re = 400$.

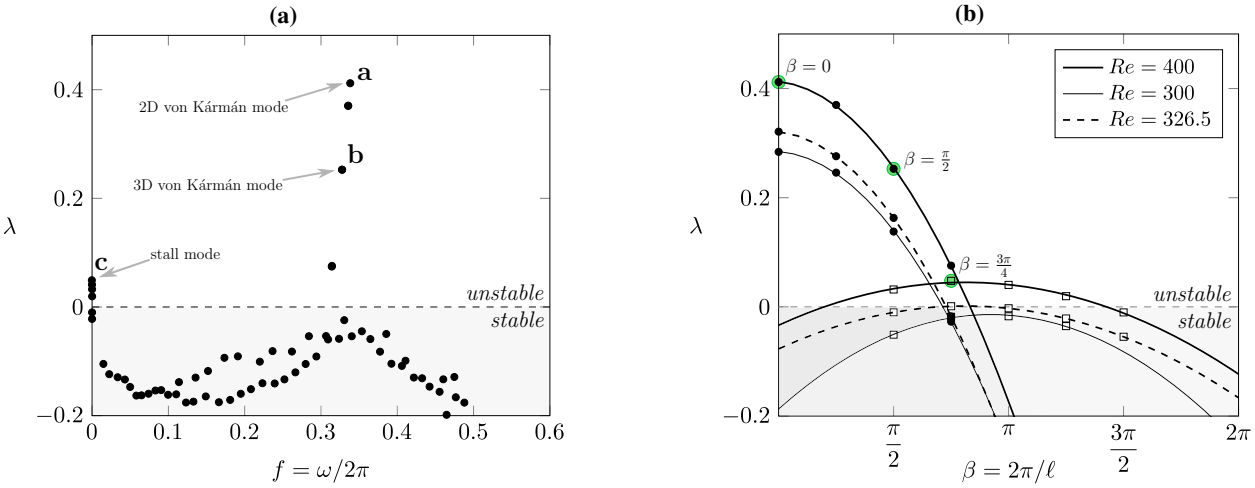

Fig. 4 (a) Spectrum relative to the base state of Fig. 3 for $\alpha = 20°$ and $Re = 400$ and (b) the growth rate as a function of the spanwise wavenumber. The bold letters in Fig. (a) and the green dots in Fig. (b) indicate the corresponding direct eigenmodes illustrated in Fig. 5.

the spanwise periodicity wavelength of an eigenmode, Figure 4(b) shows for three Reynolds numbers the growth rate of the VK and ST modes as a function of their spanwise wavenumber defined as $\beta = 2\pi/\ell$. Note that for $Re = 326.5$ the leading ST mode becomes marginally stable. The unstable global modes depicted in Fig. 4 are illustrated in Figure 5 by the real part of their streamwise velocity component. By varying the Reynolds number and the angle of attack α, we

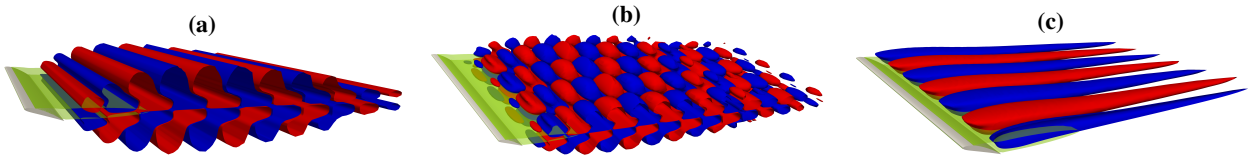

Fig. 5 Real part of the streamwise velocity for (a) the two-dimensional VK mode ($\beta = 0$), (b) the three-dimensional VK mode ($\beta = \pi/2$) and (c) the ST mode ($\beta = 3\pi/4$). The red (respectively, blue) isocontours represents positive (respectively, negative) values corresponding to one tenth of the maximal absolute value, while the opaque green isocontour represents the locus of the points where the streamwise velocity of the base flow is zero, i.e. $U = 0$.

have determined the value of *Re* for which the 2D VK mode and the ST mode become marginally stable. The results are collected in Figure 6 together with the corresponding Strouhal number. We stress that the critical Reynolds number for

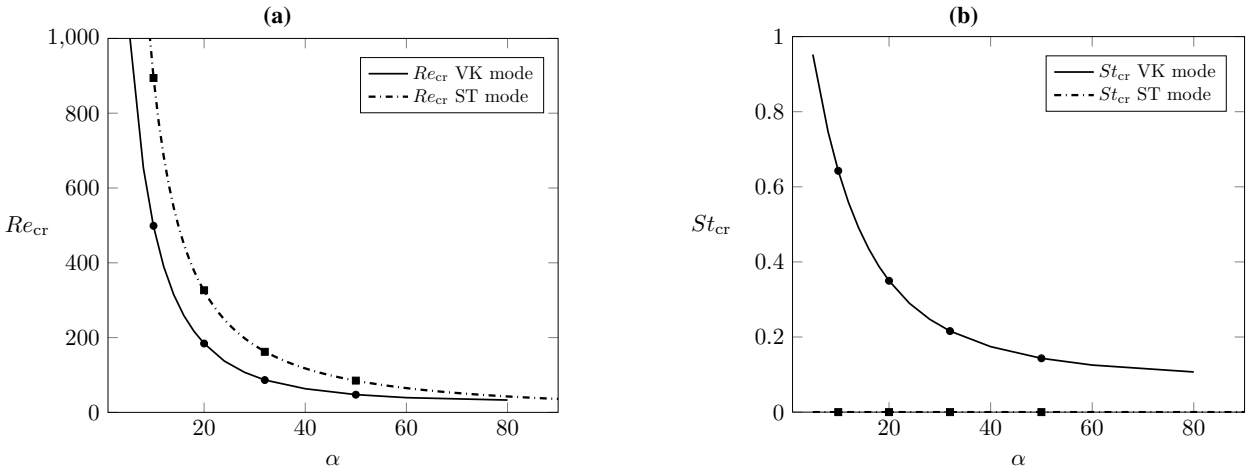

Fig. 6 (a) The emergence thresholds of the two-dimensional von Kármán (VK) mode and the stall (ST) mode in the $(\alpha - Re)$ plane and (b) the corresponding Strouhal number.

the two modes and the Strouhal number have a power-law behavior. In the whole parameter space considered in this analysis, the 2D VK mode stands as the leading global mode since the critical Reynolds number of the stall mode is always lower the one of the 2D VK one for a fixed angle of attack.

D. Sensitivity analysis

We now consider structural modifications of the stability problem arising from a steady force $\boldsymbol{F}$. The growth rate sensitivity to a force $\nabla_{\boldsymbol{F}}\lambda$ is shown in Fig. 7 for both (a) the streamwise and (b) cross-stream directions. Fig. 7(a)

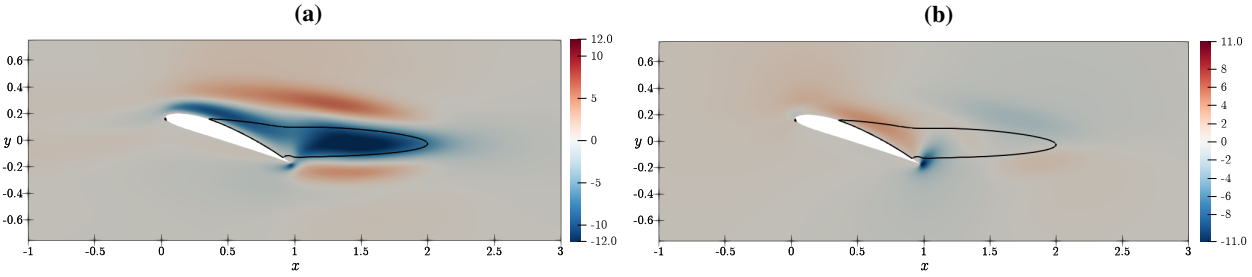

Fig. 7 Growth rate sensitivity $\nabla_{\boldsymbol{F}}\lambda$ of the 2D VK mode in (a) the streamwise and (b) cross-stream directions for $\alpha = 20°$ and $Re = 200$. The black solid line corresponds to the isocontour $U = 0$.

shows that a steady force acting inside the recirculation bubble along the streamwise direction is stabilizing since the sensitivity exhibits negative values. Furthermore, an extended region localized on the suction side is stabilizing as well. It represents a region of interest for the jet actuators arrangement. Conversely, acting on the shear zones outside the recirculation region induces a positive variation of the growth rate, i.e. $\delta\lambda > 0$. As concerns the cross-stream direction, Fig. 7(b) illustrates that the highest sensitivity is concentrated around the trailing edge, while the suction side hosts weak positive values. This suggests that adopting tangential jet actuators could be more efficient if the goal for the control is to stabilize the flow. Note that if a local force had been adopted here to interpret the sensitivity maps, the present approach would also be able to predict whether a distributed force or a non-local one have a stabilizing or destabilizing effect.

The frequency sensitivity is depicted in Fig. 8 in terms of (a) the streamwise and (b) cross-stream components. The streamwise component of the frequency sensitivity function shows that a stabilizing local force is associated with an increase of the frequency in both the separation and recirculation regions, and a slight decrease of the frequency in the outer region. Like for the growth rate, the cross-stream component is essentially concentrated around the trailing edge

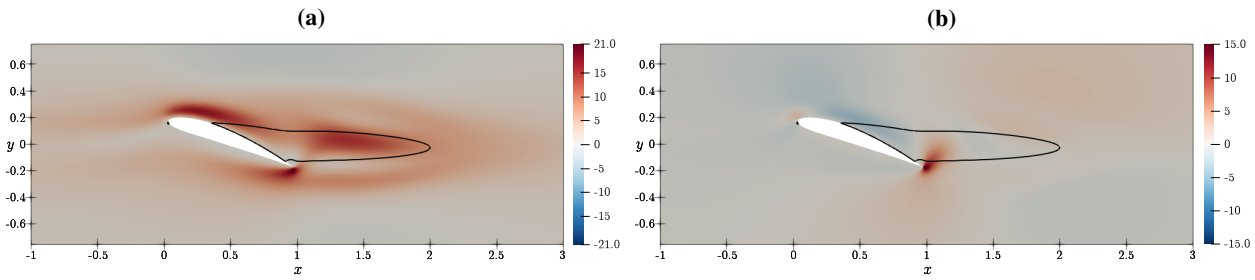

Fig. 8 Frequency sensitivity $\nabla_F \lambda$ of the 2D VK mode in (a) the streamwise and (b) cross-stream directions for $\alpha = 20°$ and $Re = 200$. The black solid line corresponds to the isocontour $U = 0$.

where a localized normal oscillator would yield an increase of the frequency. Analogously in the near proximity of the leading edge a local force would slightly increase the frequency, while in the extended region along the suction side, it would lead to a shift towards low frequencies.

Figure 9 shows the growth rate sensitivity of the stall mode (the one depicted in Fig. 5(c)) in the streamwise direction. The result shows that the location of the local steady force along the span becomes really important in a fully

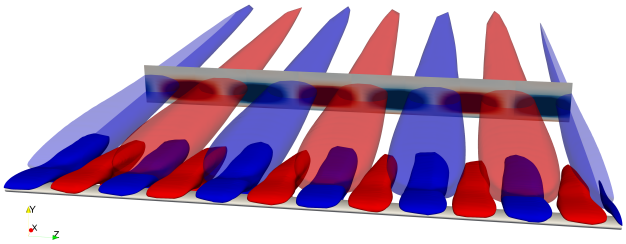

Fig. 9 Growth rate sensitivity $\nabla_F \lambda$ of the stall mode in the streamwise directions for $\alpha = 20°$ and $Re = 400$. The red (respectively, blue) isocontours represents positive (respectively, negative) values corresponding to one tenth of the maximal absolute value. The opaque isocontours illustrate the real part of the streamwise velocity for the corresponding direct stall mode, while the upstream slice depicts the associated streamwise vorticity.

three-dimensional dynamics. As shown by Marquet et al. [1], stabilizing the leading mode could not lead to a whole shift-down of the spectrum. Therefore, it is good to also consider the sensitivity information from the other global modes if the goal for the control is to stabilize all the unstable modes governing the flow dynamics.

IV. Conclusion and perspectives

With the present analysis we can numerically investigate the global mode sensitivity which is based on the evaluation of gradients through adjoint methods. This sensitivity analysis is applied to a wing modeled using a NACA 4412 airfoil and allows to predict the regions of the flow which are most sensitive to an external forcing modeling PJAs. In fact, the sensitivity to a steady force can allow for identifying where and in which directions a steady force should be applied to induce the largest stabilizing effect.

Until now, the study has been performed at low Reynolds numbers, but an extension of this approach to the turbulent regime will be provided for the H2020 Clean-Sky project PERSEUS.

Acknowledgments

This project has received funding from the Clean Sky 2 Joint Undertaking (JU) under grant agreement No 887010. The JU receives support from the European Union's Horizon 2020 research and innovation program and the Clean Sky 2 JU members other than the Union. Moreover, this research was supported by the French National Research Agency ANR (project 18-CE46-009). This work was granted access to the HPC resources of IDRIS under the allocation 2021-33A0092A06362 made by GENCI.

References

[1] Marquet, O., Sipp, D., and Jacquin, L., "Sensitivity analysis and passive control of cylinder flow," *J. Fluid Mech.*, Vol. 615, 2008, p. 221.

[2] Paul F. Fischer, J. W. L., and Kerkemeier, S. G., "nek5000 Web page," , 2008. Http://nek5000.mcs.anl.gov.

[3] Williamson, C. H. K., "Vortex dynamics in the cylinder wake," *Annual Review of Fluid Mechanics*, Vol. 28, No. 1, 1996, pp. 477–539.

[4] Strykowski, P. J., and Sreenivasan, K. R., "On the formation and suppression of vortex'shedding' at low Reynolds numbers," *J. Fluid Mech.*, Vol. 218, No. 1, 1990, pp. 71–107.

[5] Åkervik, E., Brandt, L., Henningson, D. S., Hœpffner, J., Marxen, O., and Schlatter, P., "Steady solutions of the Navier-Stokes equations by selective frequency damping," *Phys. Fluids*, Vol. 18, No. 6, 2006, p. 068102.

[6] Cunha, G., Passaggia, P.-Y., and Lazareff, M., "Optimization of the selective frequency damping parameters using model reduction," *Phys. Fluids*, Vol. 27, No. 9, 2015, p. 094103.

[7] Dijkstra, H. A., Wubs, F. W., Cliffe, A. K., Doedel, E., Dragomirescu, I. F., Eckhardt, B., Gelfgat, A. Y., Hazel, A. L., Lucarini, V., Salinger, A. G., et al., "Numerical bifurcation methods and their application to fluid dynamics: analysis beyond simulation," *Communications in Computational Physics*, Vol. 15, No. 1, 2014, pp. 1–45.

[8] Loiseau, J.-C., Bucci, M. A., Cherubini, S., and Robinet, J.-C., "Time-stepping and Krylov methods for large-scale instability problems," *Computational Modelling of Bifurcations and Instabilities in Fluid Dynamics*, Springer, 2019, pp. 33–73.

[9] Hill, D. C., "Adjoint systems and their role in the receptivity problem for boundary layers," *J. Fluid Mech.*, Vol. 292, 1995, pp. 183–204.

[10] Barkley, D., Blackburn, H. M., and Sherwin, S. J., "Direct optimal growth analysis for timesteppers," *International journal for numerical methods in fluids*, Vol. 57, No. 9, 2008, pp. 1435–1458.

[11] Farrell, B. F., "Optimal excitation of perturbations in viscous shear flow," *Phys. Fluids*, Vol. 31, No. 8, 1988, pp. 2093–2102.

[12] Giannetti, F., and Luchini, P., "Structural sensitivity of the first instability of the cylinder wake," *J. Fluid Mech.*, Vol. 581, No. 1, 2007, pp. 167–197.

[13] Bottaro, A., Corbett, P., and Luchini, P., "The effect of base flow variation on flow stability," *J. Fluid Mech.*, Vol. 476, 2003, p. 293.

[14] Barkley, D., "Linear analysis of the cylinder wake mean flow," *EPL (Europhysics Letters)*, Vol. 75, No. 5, 2006, p. 750.

[15] Sipp, D., and Lebedev, A., "Global stability of base and mean flows: a general approach and its applications to cylinder and open cavity flows," *J. Fluid Mech.*, Vol. 593, 2007, p. 333.

[16] Kitsios, V., Rodríguez, D., Theofilis, V., Ooi, A., and Soria, J., "BiGlobal stability analysis in curvilinear coordinates of massively separated lifting bodies," *J. Comput. Phys.*, Vol. 228, No. 19, 2009, pp. 7181–7196.

[17] Rodríguez, D., and Theofilis, V., "On the birth of stall cells on airfoils," *Theor. Comput. Fluid Dyn.*, Vol. 25, No. 1, 2011, pp. 105–117.